Trapping characteristics and a donor-complex (DX) model for the persistent-photoconductivity trapping center in Te-doped $Al_xGa_{1-x}As$

D. V. Lang and R. A. Logan
Bell Laboratories, Murray Hill, New Jersey 07974

M. Jaros*
Department of Physics and Astronomy, University of Massachusetts, Amherst, Massachusetts 01003
(Received 25 January 1978)

Photocapacitance measurements have been used to determine the electron photoionization cross section of the centers responsible for persistent photoconductivity in Te-doped $Al_xGa_{1-x}As$. The cross-section data, which have been obtained at various temperatures and for crystals of various alloy compositions, are fitted by a theoretical line shape that is valid for large lattice relaxation. The line shape and thermal broadening can best be fit by a binding energy of 0.10 ± 0.05 eV and a Franck-Condon energy of 0.75 ± 0.1 eV. These values are in good qualitative agreement with the large-lattice-relaxation model of persistent photoconductivity which we recently proposed. We show that the 0.10-eV binding energy is also consistent with experiments that locate this energy relative to the Fermi level. The dependence of the properties of the persistent-photoconductivity center on the donor doping of the samples leaves little doubt that this center involves a donor atom, but because the center is not effective-mass-like, we believe that it is a complex also involving another constituent. Accordingly, we designate it as a "DX" center. The anomalously-large Franck-Condon energy (Stokes shift) and apparent fact that the unoccupied state of the DX center is resonant with the conduction band, yet sufficiently localized to produce a large relaxation, are thus well established. These considerations lead us to the propose that the most likely model for DX centers in $Al_xGa_{1-x}As$, and perhaps in other compound semiconductors as well, is a complex involving a donor and an anion vacancy. We show that such a model is qualitatively consistent with the overall trends in persistent-photoconductivity behavior observed in a variety of III-V and II-VI semiconductors.

I. INTRODUCTION

In this paper we will discuss the thermal and optical properties of the persistent-photoconductivity center in Te-doped $Al_xGa_{1-x}As$. The dominant features of this type of defect are: (a) an apparently enormous Stokes shift (thermal depth from the conduction band ~0.1 eV, optical depth ~1 eV), and (b) a very small thermally activated electron-capture cross section ($<10^{-30}$ cm^2), for temperatures below about 77 K. These features could be semiquantitatively explained by a somewhat unorthodox configuration coordinate (CC) model which postulated a lattice relaxation that was very large for such an apparently shallow center, i.e., the Franck-Condon energy d_{FC} was proposed to be much larger than the apparent electronic binding energy E_0.[1] We will present here temperature-dependent optical data for this center which lend further support to the lattice-relaxation model of Ref. 1 and leave little doubt as to its overall qualitative validity.

The verification of this model, however, raises more questions than it answers. For within the framework of the traditional understanding of point defects in semiconductors, based on the effective-mass theory, the model of Ref. 1 is physically untenable. The fact that $d_{FC} \gg E_0$ is hard to explain, since for all cases where it has been measured, d_{FC} is some fraction, typically 0.1–0.5, of E_0. Second, the CC model of Ref. 1 requires that the defect charge density be sufficiently localized to produce a large lattice relaxation even when the state is resonant with the conduction band. This is even harder to explain, since the conventional wisdom has it that such resonant states are highly delocalized, and hence the electron-lattice interaction could not possibly produce such a large relaxation. We will show that a proper view of the origin and structure of defect wave functions can resolve these apparent contradictions.

The dependence of the properties of the persistent-photoconductivity center on the donor doping of the samples leaves little doubt that this center involves a donor atom. But because the center is not effective-mass-like and because its concentration is not always a fixed fraction of the donor concentration, we believe that is is a complex involving another constituent as well. Accordingly we designate it as a DX center. Based on the current theoretical understanding of deep levels in semiconductors, we will present arguments which we believe show that DX centers are most likely complexes involving a donor atom and an anion vacancy, e.g., Te-V_{As} for Te-doped

$Al_xGa_{1-x}As$.

In Sec. II we will discuss the experimental methods and in Sec. III we will present the experimental results. Section IV is a brief discussion of the optical-line-shape theory used to fit the data. Finally, the resolution of the theoretical inconsistencies mentioned above and our proposal for the microscopic structure of *DX* centers are presented in Sec. V. The paper is summarized in Sec. VI.

II. EXPERIMENTAL METHODS

A. Crystal growth and sample preparation

The $Al_xGa_{1-x}As$ samples used in this study were grown on n^+ GaAs substrates by liquid-phase epitaxy (LPE) from gallium solution at 850 °C. Schottky barriers were fabricated on single n-type epitaxial layers by evaporating a semitransparent (~10% transmission) gold film through a mask with 250- and 500-μm diam circular openings. Some of the n layers were covered with a second p-type epitaxial layer doped with Ge ($N_A - N_D = 2\times10^{18}$ cm^{-3}). The p-type layer was either of the same aluminum content x (for p-n homojunctions) or of pure GaAs (for single p-n heterojunctions). These p-n junctions were formed into mesa diodes by applying conventional metallized Ohmic contacts, sand blasting, and chemical etching. They were then mounted on TO-18 headers with leads attached to the metallized Ohmic contacts by thermocompression bonding. Some of the p-n junctions were mounted on edge so that the junction space-charge layer could be uniformly illuminated through the substrate. In a few of the samples the substrate was removed by selective chemical etching in order to avoid the effects of the substrate absorption for $h\nu > 1.4$ eV. For $h\nu < 1.3$ no essential differences were seen in the experiments performed on the three types of samples—homojunctions, heterojunctions, or Schottky barriers. The predominant dopant in the n-type $Al_xGa_{1-x}As$ epitaxial layer was

$$\text{Te } (5\times10^{16} < N_D - N_A < 2\times10^{18} \text{ cm}^{-3}),$$

although a few preliminary results were obtained on samples doped with Se, Si, and Sn. Unless otherwise noted, all results in this paper will be for the Te-doped samples.

B. Capacitance spectroscopy techniques

The samples were studied by various forms of capacitance spectroscopy, namely, deep-level transient spectroscopy[2,3] (DLTS) and thermally stimulated capacitance[2] (TSCAP) for the thermal-emission and capture data, and photocapacitance[2] for the optical cross-section data. The net shallow-level doping concentration was measured by a Miller feedback profiler.[2,4] These techniques are especially well suited for the measurement of deep-level concentrations. Thus, there is no doubt that the thermal and optical data relate to the same center, since this center dominates the behavior of our samples.

In order to explain how the data in Sec. III were taken, we show typical DLTS and TSCAP curves in Figs. 1(a) and 1(b), respectively. As is well known,[2,3] these techniques correspond to the same physical phenomena—thermal emission or capture of trapped carriers in the junction space-charge layer, observed on different time scales. Thus, the DLTS peaks in Fig. 1(a) correspond to thermal electron emission following a zero-biasing voltage pulse (negative peak) and electron capture following a forward-bias injection pulse (positive peak), both with a 2.7-msec time constant. The TSCAP data in Fig. 1(b), on the other

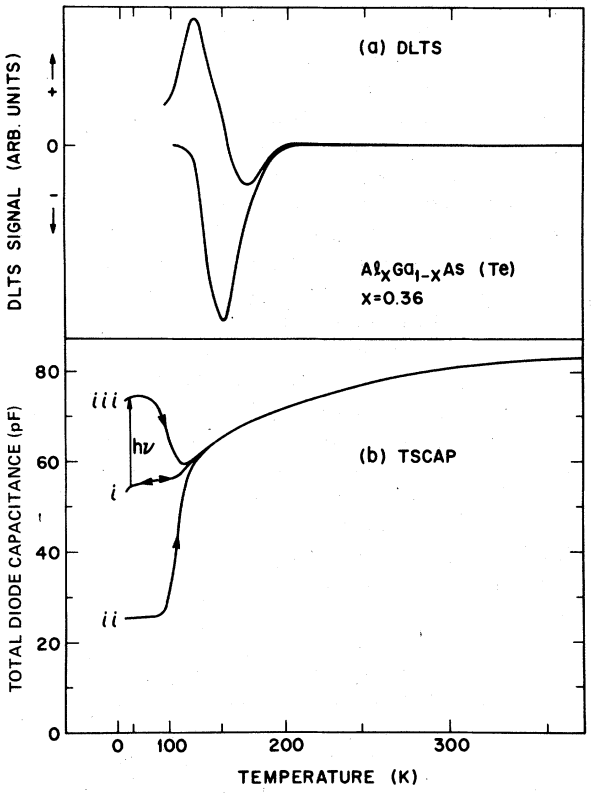

FIG. 1. DLTS and TSCAP data for a typical sample of Te-doped $Al_xGa_{1-x}As$ with $x = 0.36$. The DLTS spectra correspond to a rate window of 366 sec^{-1}; the TSCAP heating rate was ~1 K/sec. Increases in C correspond to fewer trapped electrons, while decreases in C imply more trapped electrons. The photocapacitance transition is indicated by the arrow labeled $h\nu$.

hand, correspond to time constants of the order of seconds. This explains the shift of the DLTS data to higher temperatures. The positive going TSCAP step, corresponding to initial condition (*ii*) (defined below) is the same physical phenomenon (thermal electron emission) as the negative DLTS peak. From the magnitude of this TSCAP step one can calculate the concentration of deep levels which are emitting electrons with rates of the order of seconds in the temperature range of the step. Similarly, the negative going TSCAP step corresponding to initial condition (*iii*) (also defined below) arises from the same effect as the positive DLTS peak. We have found that this is due to electron capture in the case of DX centers in $Al_xGa_{1-x}As$.

Usually a positive DLTS peak or a negative TSCAP step is due to minority-carrier emission (holes in this case). However, the fact that initial condition (*iii*) can be established in n-type Schottky barriers by illumination with photons of energy as low as 0.6 eV totally rules out the possibility of hole emission in this temperature range, since $\gtrsim$1.5 eV light would be needed to empty hole traps close enough to the valence band to emit holes at the same temperature as the positive DLTS peak. The fact that electron capture can give a signal that looks so much like hole emission is due to the peculiar nature of the DX center, i.e., its electron-capture cross section is very small and thermally activated at low temperatures.[1]

Since most of the data in this paper have been obtained by the techniques shown in Fig. 1(b), it is important to consider in some detail the procedures used in establishing the initial conditions for the three $C(T)$ curves. Curve (*i*) is the steady-state zero-bias capacitance recorded as a function of temperature. This curve is reversible for increasing or decreasing temperature scans. Curves (*ii*) and (*iii*), on the other hand, are irreversible thermal scans corresponding to initial conditions at the lowest temperature of completely filled or completely empty DX centers, respectively. Initial condition (*ii*) is obtained by cooling the sample from about 200 K to about 50 K with +1 V bias. This bias corresponds to a narrowing of the junction space-charge layer so that nearly all DX centers (which are donors in $Al_xGa_{1-x}As$[5]) are below the Fermi level, tend to be filled with electrons, and hence are neutral. At the lowest temperature, the bias is returned to 0 V, where the filled DX centers in the space-charge region constitute a nonequilibrium state which is metastable because the electron thermal-emission rate is vanishingly small at 50 K. Thus, as shown in Fig. 2(a), the space-charge layer of width W_{ii} is made up only of ionized "normal"

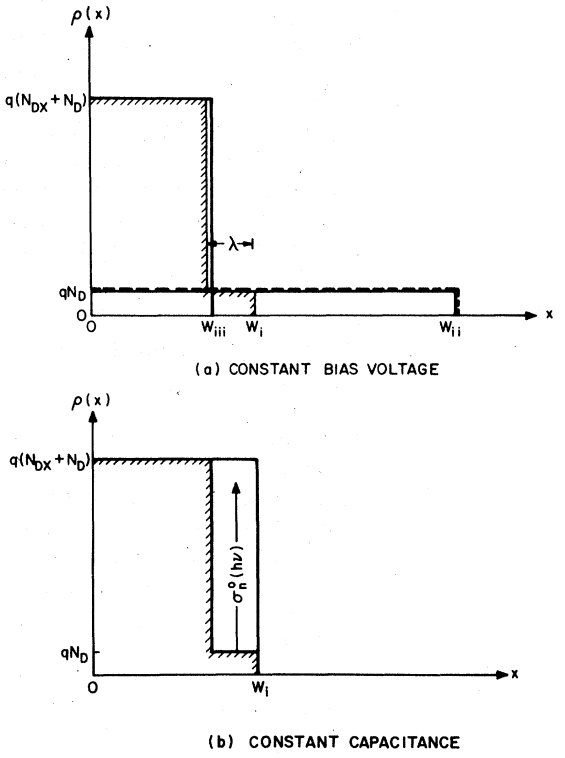

FIG. 2. Charge density vs distance in the abrupt-depletion approximations (a) for the junction space-charge layer corresponding to the three TSCAP initial conditions in Fig. 1, and (b) for the constant-capacitance condition of the photoionization measurements.

donors of net concentration N_D. When the temperature is increased to the vicinity of 100 K, the DX centers begin to thermally emit their trapped electrons and hence become positively charged. Since $N_{DX} \gg N_D$ in most of our samples, this corresponds to a drastic rearrangement of the space charge at constant bias which finally results in the equilibrium width W_i, shown in Fig. 2(a) as the step-wise charge distribution with shaded boundaries. The step at $W_i - \lambda$ corresponds to the point where the DX energy level passes through the Fermi level in the edge region of the space-charge layer.[2,6] Thus between 0 and $W_i - \lambda$, the DX centers are above E_F and are empty in equilibrium so that the positive space charge is $q(N_{DX} + N_D)$; In the edge region from $W_i - \lambda$ to W_i, the energy level of the DX centers is below the Fermi level so that the equilibrium space charge is only qN_D. The steady-state capacitance change of curve (*i*) as a function of temperature corresponds primarily to the temperature dependence of the Fermi level, and consequently of λ. As λ changes with temperature at constant-bias voltage, the space-charge distribution, and hence W_i in Fig. 2(a), must change accordingly.

Initial condition (*iii*) in Fig. 1(b) corresponds to all DX centers empty. This is illustrated in Fig. 2(a) with the space-charge distribution $q(N_{DX}+N_D)$ from 0 to W_{iii} with no edge region. Condition (*iii*) is obtained at low temperature from the steady-state condition (*i*) by emptying the DX centers either *optically*, by exciting the electrons to the conduction band, or *electrically*, by recombination of the electrons with injected holes under forward bias. The optical emptying path is illustrated in Fig. 1(b) and is utilized in the following photocapacitance method to measure the electron photoionization cross section $\sigma_n^0(h\nu)$.

In the low-temperature limit, where thermal-emission and capture rates are negligible, the concentration of occupied DX centers $n_{DX}(t)$ is given by[2]

$$n_{DX}(t)=N_{DX}\exp(\sigma_n^0\Phi t)\,, \tag{1}$$

where Φ is the optical intensity in photons/cm^2 sec. In the limit where $N_{DX}\gg N_D$, the capacitance is a complicated function of $n_{DX}(t)$; thus the time dependence of C from (*i*) to (*iii*) in Fig. 1(b) is far from the simple exponential relationship of Eq. (1). This is dramatically illustrated by the typical photocapacitance transient at constant bias voltage shown in Fig. 3. If, however, instead of measuring the capacitance, we monitor the bias voltage change necessary to maintain a constant capacitance, the resulting voltage transient has the simple exponential form of Eq. (1). This virture of constant capacitance measurements in the concentrated deep-level limit was first pointed out by Goto *et al.*[7] We use the constant-depletion mode of a Miller feedback profiler[4] to record the constant-capacitance data.

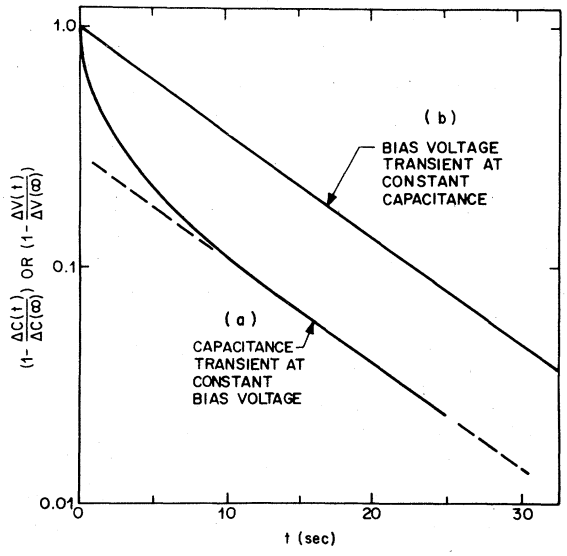

FIG. 3. Transients due to the photoionization of DX centers as observed for the same experimental conditions by two methods of measurement: (a) capacitance transient at constant bias and (b) bias-voltage transient at constant capacitance.

The experimental sequence is as follows. The sample is first cooled at zero bias to reach condition (*i*), and then the profiler is switched to the constant-depletion mode with the depletion depth set at W_i. When the monochromator is turned on, the DX centers in the edge region are emptied according to Eq. (1), as shown in Fig. 2(b). The photoionization transient is measured by recording the feedback bias voltage as shown in Fig. 3. The optical cross section σ_n^0 can then be obtained from the time constant of the voltage transient if Φ is known. In these experiments the light source was a Bausch and Lomb high-intensity monochromator. The monochromator output was measured with a calibrated thermopile.

A peculiar property of DX centers, which is the cause of persistent photoconductivity,[1] is that when emptied at low temperatures it is impossible to refill the centers without warming the sample. The thermal barrier due to lattice relaxation essentially stops all electron capture below about 77 K, and the fact that the empty DX state is not in the gap makes it impossible to optically refill the level from the valence band. Thus in order to measure σ_n^0 at a different photon energy after the system is in state (*iii*), it is first necessary to warm the sample to some temperature above the negative-going electron-capture TSCAP step in Fig. 1(b). As shown in Ref. 1, this electron-capture step is the same physical phenomenon as the thermal quenching of persistent photoconductivity. State (*iii*) in Fig. 1(b), therefore, corresponds to the persistent-photoconductivity state seen by photo-Hall or photoconductivity measurements.[1] As a consequence, in the measurements of $\sigma_n^0(h\nu)$, which are discussed in Sec. III, the temperature cycle from the measurement temperature T up to 150–200 K along curve (*iii*) and back to T along curve (*i*) is required for each value of $h\nu$.

C. Determination of concentrations

The capacitance values corresponding to conditions (*i*), (*ii*), and (*iii*) in Fig. 1(b) can be put on a more quantitative basis in order to determine the DX center and net normal-donor concentrations. The necessary relationships are based on a double integral of Poisson's equation giving the voltage drop across a spatially uniform charge distribution ρ of width x as $\rho x^2/2\epsilon$, where ϵ is the dielectric constant of the medium. The step-function charge distributions in Fig. 2 are based on the so-called abrupt-depletion approximation which is

reasonably accurate for all conditions except forward bias.[6] From Fig. 2 we have

$$2\epsilon(V_{bi}+V)=q[W_I^2N_D+(W_I-\lambda)^2N_{DX}], \quad (2)$$

$$2\epsilon(V_{bi}+V)=qW_{II}^2N_D, \quad (3)$$

$$2\epsilon(V_{bi}+V)=qW_{III}^2(N_{DX}+N_D), \quad (4)$$

where V_{bi} is the so-called built-in potential which is on the order of the band gap, and V is the bias voltage. The depletion-layer width W is related to the capacitance by

$$C=\epsilon A/W, \quad (5)$$

with A the area of the junction. Since the capacitance values in Fig. 1(b) all correspond to the same bias voltage, Eqs. (2)–(4) are all equal to each other. Thus from Eqs. (3) and (4) we have

$$\frac{N_{DX}}{N_D}=\left(\frac{C_{III}}{C_{II}}\right)^2-1, \quad (6)$$

From the double integral of Poisson's equation in the uniform concentration limit, we have

$$\lambda=(2\epsilon\phi_{FT}/qN_D)^{1/2}, \quad (7)$$

where $\phi_{FT}=(E_F-E_T)/q$, and E_T is the energy of the deep level of interest. For the DX-center case $E_T=E_C-E_0$, where E_0 will be defined in Sec. IV. Thus by using the value of N_{DX}/N_D from Eq. (6), the fact that the bias voltage is zero for the case of Fig. 1(b) and the experimental value of C_{II}, we can solve Eq. (2) to obtain λ and ϕ_{FT}. For the data in Fig. 1(b), we find $N_{DX}/N_D=8$ with $N_{DX}+N_D \sim 10^{18}$ cm^{-3}, and $\phi_{FT}=44$ mV at 100 K. The charge-density diagrams in Fig. 2 correspond to these values.

The steady-state capacitance change between 100 and 300 K can also be explained quantitatively by Eqs. (2)–(4). As the temperature increases from 100 K, the Fermi level drops in the gap so that ϕ_{FT}, and hence λ, become smaller. Thus, from Eq. (2), W must become smaller to maintain the same voltage drop. In the limit of $\lambda \to 0$, $W \to W_{III}$ in Eq. (4). As we can see in Fig. 1(b) this approximates the experimental situation. We expect and observe that the higher-temperature capacitance is actually somewhat larger than C_{III} since the band gap, and hence V_{bi}, decreases with increasing temperature. Another effect will cause the room-temperature capacitance to be given by Eq. (4) even if $\phi_{FT} \neq 0$; namely, at approximately 250 K the extrapolated thermal-emission rate e_n^t from the DX center[1] becomes equal to $\omega_{rf}=2\pi \times 10^6$ sec^{-1}, corresponding to the capacitance measurement frequency of 1 MHz. In this case, when the deep-level occupation can follow the measurement frequency, the capacitance is given by Eq. (4), which includes both the shallow- and deep-level concentrations as if λ were zero, even if it actually is not.[8] Normally, the transition from the high- to the low-frequency limit is accompanied by a well-defined step in the C vs T curve, and is the basis of the admittance spectroscopy technique.[9] For the DX center, however, no such step is seen near 250 K. Apparently, ϕ_{FT} is close enough to zero at 250 K and/or the $\omega_{rf} \sim e_n^t$ step is broad and small enough so as not to be noticeable.

Note that the very fact that $C(T)$ gradually decreases from 300 to 100 K is unusual, and relates to the DX center being the dominant donor in these samples. Our measurements on samples with normal donors of approximately the same depth (~0.1 eV), e.g., n-GaP, show a relatively temperature-independent $C(T)$ curve down to about 80–100 K. At that point the capacitance abruptly drops to zero because either e_n^t of the donors or the device RC time constant can no longer follow ω_{rf}. Most ~0.1-eV-deep levels can follow ω_{rf} above 100 K and hence contribute to the space-charge-layer capacitance, even if the carrier concentration in the bulk is much lower than N_D-N_A, i.e., capacitance measures N_D-N_A, not n. For the class of $\lesssim$0.1-eV-deep donors the gradual $C(T)$ curve in Fig. 1 is *only* seen for DX centers; this is further evidence that the DX thermal-emission depth is considerably greater than its equilibrium depth.[1] Indeed, the edge-region photocapacitance technique used here [see Fig. 2(b)] would not be possible for normal donors because the recapture of electrons in the edge region is typically much faster than the photoionization rate for all but the most intense light sources, e.g., tunable ir lasers. The fact that the DX center is the cause of persistent photoconductivity, i.e., has a vanishingly small electron-capture rate at 50 K, is the only reason why the somewhat unusual techniques used here work at all.

III. EXPERIMENTAL RESULTS

A. Optical line shape

The electron-photoionization cross section $\sigma_n^0(h\nu)$ measured by the constant-capacitance bias-voltage-transient technique of Figs. 2(b) and 3 is shown in Fig. 4 for an $x=0.37$ Schottky-barrier sample with the substrate removed. These data were taken for two temperatures, 44 and 78 K. The solid lines in Fig. 4 are a theoretical fit according to the phonon-broadened line-shape theory to be outlined in Sec. IV. The small temperature range of 44–78 K was dictated by the experimental constraint that the thermal-emission and capture rates be small compared to the optical-emission rate. The modest thermal broadening in Fig. 4 is actually quite large for such a small temperature

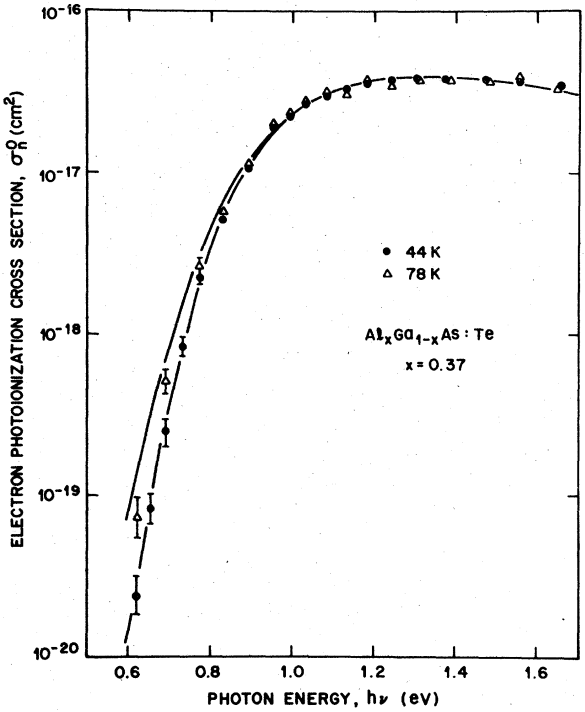

FIG. 4. Normalized electron-photoionization cross-section $\sigma_n^0(h\nu)$ for two temperatures. The solid lines are theoretical fits to the data.

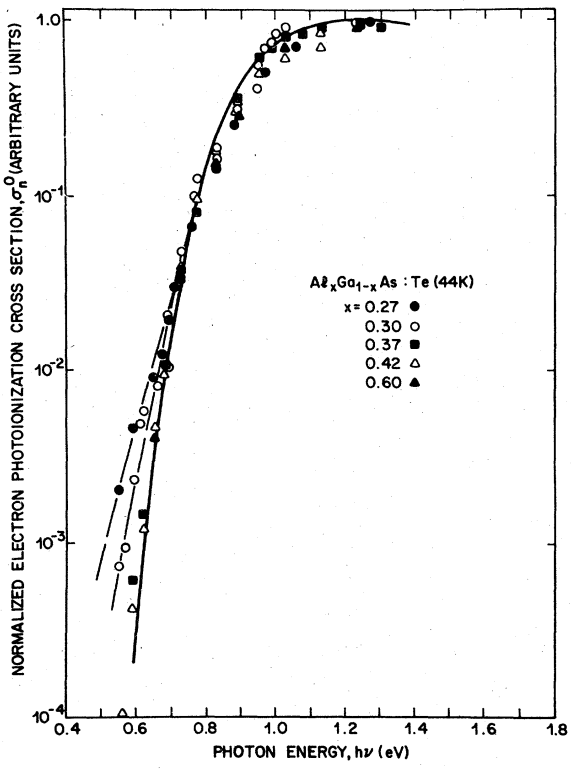

FIG. 5. Normalized electron-photoionization cross-section $\sigma_n^0(h\nu)$ at 44 K for five samples with different Al fractions. The heavy curve is the same theoretical fit as in Fig. 4.

rise and, as we will discuss in Sec. IV, verifies the qualitative features of the large-lattice-relaxation model of Ref. 1. The maximum cross section of 4×10^{-17} cm^2 is typical of other deep levels as reported in the recent review by Grimmeiss.[10]

Figure 5 shows data from five samples of different aluminum content ($0.27 \leq x \leq 0.60$) all taken at 44 K. We have normalized all the data to unity at 1.2 eV without having measured the absolute cross-section changes from sample to sample. The heavy line drawn through the data is the 44-K theoretical fit shown in Fig. 4. The lighter lines for $x=0.27$ and $x=0.30$ are not fits but are intended to show how these samples, well into the direct-gap composition range, have distinguishable shifts in the threshold region for $\sigma_n^0 < 10^{-2}\sigma_{max}$. As we will discuss in Sec. IV, these weak tails at low values of $h\nu$ most likely correspond to transitions to the low density of states at Γ. It is noteworthy that the remainder of the curves shows essentially no consistent variation with crystal composition. Indeed, the three curves for $x=0.37$, 0.42, and 0.60 are practically indistinguishable.

B. Variations of DLTS spectra

The small sample-to-sample variations that are seen in Fig. 5, other than the direct-gap tails, may be attributable to the fact that the DX center does not seem to be a single well-defined center, but rather a closely related family of defects with a slight spread in binding energies. The range of possible Te-related DX centers is shown in the selected DLTS electron-emission spectra shown in Fig. 6. Note that some samples actually show two resolved DLTS peaks, while most show a single peak of varying width located somewhere between the extremes of the double-peak examples. The range of peak positions in Fig. 6 corresponds to a shift of about 60 meV in the thermal-emission activation energy of ~0.3 eV. There is no systematic correlation of these peak positions, and hence of thermal-emission energies, with mixed crystal composition. Apparently, the dominant type of DX center in any given sample is determined more or less at random. The only possible correlation with x is that the very few double-peak examples seem to occur more readily at the extremes of the composition range, i.e., in the $x=0.20$–0.30 or $x \geq 0.6$ range. Perhaps the relative probabilities of particular Ga or Al arrangements around the defect play a role in the slight shifts of its properties.

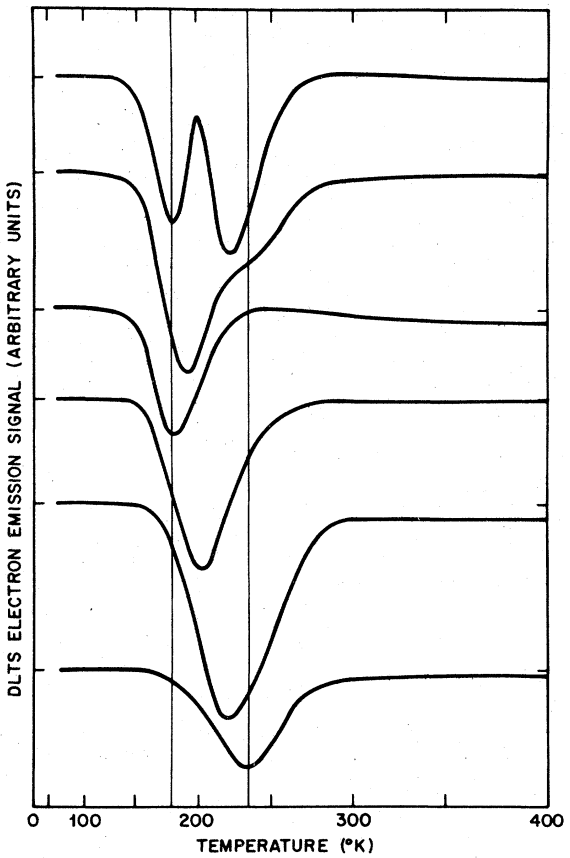

FIG. 6. DLTS spectra of the DX centers in six Te-doped $Al_xGa_{1-x}As$ samples selected to show the typical range of peak positions and line shapes commonly observed. The rate window was 3.7×10^5 sec^{-1}, with a 2-V reverse bias and a 3-V majority-carrier pulse of 10-μsec duration.

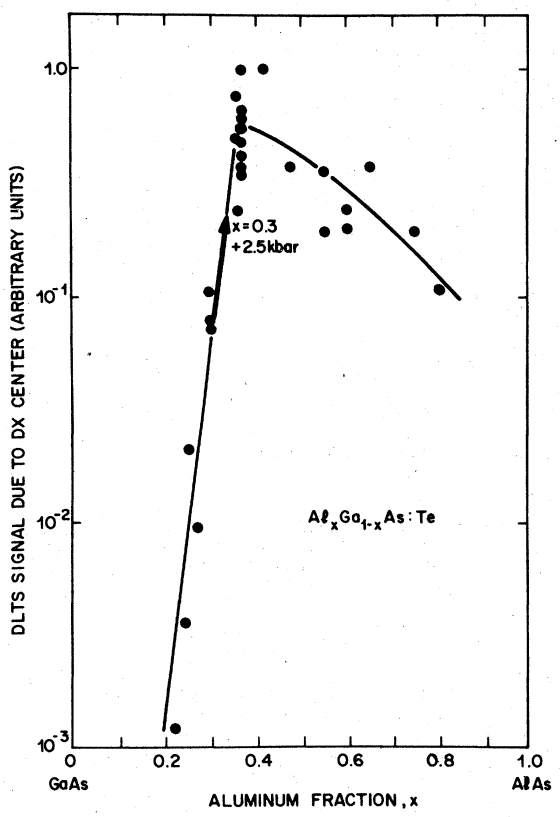

FIG. 7. DLTS signal magnitude due to DX centers in various $Al_xGa_{1-x}As$ samples vs the aluminum fraction x of the sample under the same conditions as the spectra in Fig. 6. The heavy arrow indicates the signal increase in an $x=0.3$ sample induced by the application of a 2.5 kbar stress. The discontinuous drip in DLTS signal below $x=0.36$ corresponds to E_0 crossing the Fermi level, as explained in the text.

C. DX signal versus x and stress

Let us now discuss a set of data which are valuable in assessing the reasonableness of the energies to be determined in Sec. IV from the optical fit. These data, as shown in Fig. 7, are the magnitudes of the DLTS signal due to DX centers in a large number of samples of various Al content. Note that there is quite a bit of scatter in the points. This corresponds to fluctuations in the N_{DX}/N_D ratio from sample to sample. In fact, using the procedure of Eq. (6) we find the N_{DX}/N_D ratio to be typically of the order of 10 but to vary from less than 1 to more than 30 in different samples. This variation has only a modest correlation with x, i.e., the lower N_{DX}/N_D values tend to occur for higher Al fractions, as seen in Fig. 7.

The precipitous drop in DLTS signal below $x=0.35$ is not due to a drop in DX concentration, however. This is shown by stress measurements. The y axis of the heavy arrow in Fig. 7 corresponds to the 3× increase in DLTS signal induced in an $x=0.3$ sample by the application of 2.5 kbar of stress; the x axis of this arrow indicates the composition change which would give rise to the same shift of the Γ minimum as does 2.5 kbar of hydrostatic stress. A similar effect was seen at $x=0.25$, but at $x=0.37$ the same level of stress produced no effect. Thus the DLTS signal is affected by stress only in the exponential-drop-off region of $x<0.35$.

The stress was applied to mesa diodes perpendicular to the junction plane; thus the sample dimension along the stress direction was considerably smaller than in the perpendicular dimension, so that the stress could be considered essentially hydrostatic. Under these conditions the major change induced by the stress is to raise the Γ and L conduction-band minima by 12.6 and 5.5 meV/kbar, respectively, and to lower the X minimum by 1.5 meV/kbar.[11] Since such an effect obviously cannot change the DX concentration, it must have

changed the DX occupation. This could only happen if the energy level of the DX center were above E_F in the $x < 0.35$ composition range, so that it would be only partially occupied during the majority-carrier pulse used to initiate the DLTS signal. The large signal change between $x = 0.35$ and $x = 0.22$ can be readily explained by an $\exp[-(E_{DX} - E_F)/kT]$ Boltzmann factor if E_F more or less follows the Γ minimum while $E_{DX} \cong E_X - E_0$ roughly follows the high-density-of-states X minimum E_X. The data in Fig. 7 can thus be interpreted as showing that E_{DX} crosses E_F for $0.32 < x < 0.35$ and more or less follows the X minimum in the direct-gap region (see Fig. 9). Also, this crossing point corresponds to $\phi_{FT} = 0$ so that $\lambda = 0$; indeed, we see no edge effects in the $C(T)$ curve for $x < 0.35$, as expected.

D. Donor doping effects

One of the most important observations concerning the DX-type centers is that they depend strongly on the concentration and chemical species of the donor added during LPE crystal growth.[1,5] First, the DX concentration depends nearly linearly on the donor concentration.[5] Despite some scatter in the data, this proportional relationship can be seen relative to both $N_D - N_A$ (determined by C-V or Hall measurements) and the amount of Te added during crystal growth.

Even if such concentration data leave one unconvinced as to the "D" of DX centers, the dramatic shifts induced by changing the chemical type of donor should leave no doubt that DX centers involve donor atoms as a constituent. We have examined several samples having n layers doped with Se, Si, Sn (or undoped) instead of the Te doping which all of our other results are based. A complete treatment of the various dopants is planned, but the preliminary data can be briefly summarized as follows. The samples doped with Se show behavior such as in Fig. 1, which is essentially identical to that of the Te-doped samples. The Si- and Sn-doped samples, on the other hand, are very different, both from Te and Se, and from each other. For example, the DLTS spectra of Sn-doped samples always show two peaks. With the same rate window (3.7×10^5 sec^{-1}) as the Te data in Fig. 6, the Sn-doped spectra have a small peak ($N_{DX} \ll N_D$) at ~245 K and a very large peak ($N_{DX} > N_D$) at about 130–140 K. The TSCAP curves, such as in Fig. 1(b), are also very different for Sn doping, i.e., the negative step from C_{iii} occurs at about 40 K, indicating a smaller barrier to electron capture than in the Te case. In general, the Sn-related DX center appears to be somewhat closer to the conduction band than the Te- or Se-related centers. The Si-related DX center is even deeper than the Te and Se centers, with the positive TSCAP step from state (i) at ~160 K and the negative step from state (iii) at ~140 K.

The unknown background donor, which is always present in the mid-10^{16}-cm^{-3} range in our samples, does not produce any of the effects reported above. Nonintentionally doped samples show no DLTS peaks in the region where the peaks due to DX centers appear, and, in addition, do not appear to exhibit persistent photoconductivity or show the qualitative TSCAP behavior of Fig. 1(b). This might mean either that the DX concentration depends nonlinearly on the donor concentration, in spite of our concentration data, or that the background donor is *not* Te, Se, Sn, or Si, but another element—perhaps C—which does not produce a DX center with states in the gap. The suggestion of C as the background donor in $Al_xGa_{1-x}As$ is not unreasonable, since the LPE growth boat is constructed from graphite.

IV. THEORETICAL FIT OF THE PHOTOIONIZATION DATA

The experimental results of a photocapacitance or optical-absorption study can be presented in terms of the normalized cross section σ per incident photon of energy $h\nu$, as in Eq. (1) and Figs. 4 and 5. It is our prime task to find a link between the characteristic properties of $\sigma(h\nu)$ and the quantum-mechanical parameters associated with a particular defect. In the present study, we will adopt a recently developed[12] approach which has been successfully applied to a number of deep-level spectra. Accordingly, we will restrict ourselves to a brief outline of the most important considerations particularly relevant to the problems we are trying to solve here.

In the absence of an electron-phonon interaction, it is a standard approximation to write the cross section σ as

$$\sigma(h\nu) = \frac{\text{const}}{h\nu} \sum_{n,\vec{k}} |\langle \psi | \exp(-i\vec{k}_\lambda \cdot \vec{r}) \vec{\epsilon}_\lambda \cdot \vec{p} | \Phi_{n,\vec{k}} \rangle|^2 \times \delta(\epsilon_0 + E_{n,\vec{k}} - h\nu) , \quad (8)$$

where $\vec{k}$ is the wave vector of the radiation field and λ is the polarization direction. In the usual dipole approximation we have $\exp(-i\vec{k}_\lambda \cdot \vec{r}) \sim 1$. The momentum matrix element in Eq. (8) really indicates an average over all degenerate initial and final states. ϵ_0, $E_{n,\vec{k}}$, and $\Phi_{n,\vec{k}}$ stand for the impurity energy, band energy, and wave function associated with a band n and reduced wave vector $\vec{k}$, respectively. ψ represents the impurity wave function.

In the event of strong coupling between the impurity and lattice, the transition probability can be expressed following the model of Huang and Rhys.[13] In this model, the equations for the electronic and phonon functions separate. Only the electron-phonon interaction which is linear in the lattice coordinates is included. The cross section σ becomes

$$\sigma(h\nu) \sim \frac{1}{h\nu} \sum_{n,\vec{k}} |\langle \psi | \exp(-i\vec{k}\cdot\vec{r})\vec{\epsilon}_\lambda \cdot \vec{p} | \Phi_{n,\vec{k}} \rangle|^2 J_{n,\vec{k}}, \tag{9}$$

where the function $J_{n,\vec{k}}$ carries the information about the vibrational states and for the model in question can be evaluated exactly.[14] For strong electron-phonon coupling, the expression for $J_{n,\vec{k}}$ simplifies to

$$J_{n,\vec{k}} = (\pi U)^{-1/2} \exp\{-[h\nu - (|E_n| + E_{n,\vec{k}})]^2/U\},$$

where

$$U = 2S(\hbar\omega)^2/\tanh(\hbar\omega/2kT). \tag{10}$$

Here $\hbar\omega$ refers to the phonon energy, k is the Boltzmann constant, S is the Huang-Rhys factor, and the terms $S\hbar\omega = d_{FC}$ and $E_n = E_0 + d_{FC}$ are defined in the configuration coordinate (CC) diagram shown in Fig. 8. The preexponential term in Eq. (10) obviously does not affect the shape of the optical cross section, and for our purposes can be omitted.

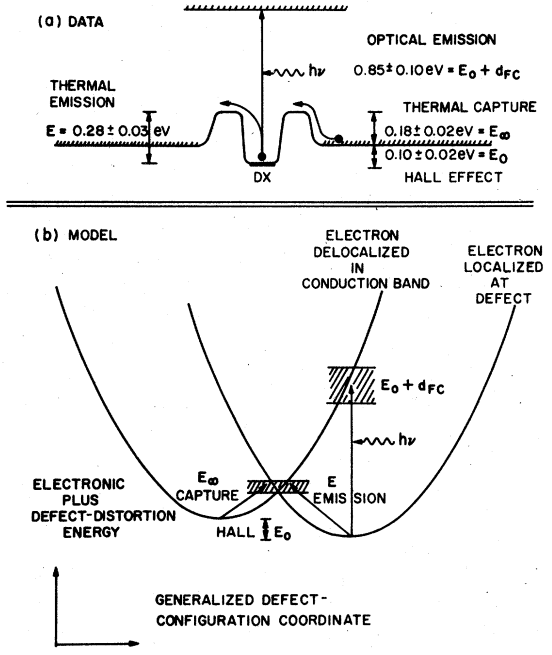

FIG. 8. (a) Summary of the experimentally determined thermal and optical energies for the DX center in Te-doped $Al_xGa_{1-x}As$. (b) CC diagram constructed to fit the data. The ranges of uncertainty in the data are shown as shaded regions.

In Ref. 12 a series of simplifying approximations were introduced which, for a sufficiently localized ψ, allow one to express Eq. (9) in the form

$$\sigma(h\nu) \sim \frac{1}{h\nu} \int_0^\infty dE\, \rho(E) \times \left| \frac{(1 \pm \eta)E^{1/2}}{|E_n| + E} + \frac{(1 \mp \eta)\sqrt{E_F}}{|E_n| - E - (E_g + E_A)/2} \right|^2 \times U^{-1/2} \exp -\left(\frac{[h\nu - (|E_n| + E)]^2}{U} \right), \tag{11}$$

where $\rho(E)$ represents the density of electron states, E_F is the free-electron Fermi energy, E_g is the forbidden band gap, and E_A is the average or Penn gap. The function $\eta(E)$ interpolates between its apparent values at $E = 0$ and $E \to \infty$, and was chosen simply as $\eta(E) = \exp(-2E/E_A)$. The required choice of + or − depends on the nodal character of ψ and corresponds to valence-band-like or conduction-band-like deep states for the upper and lower signs, respectively. In addition, $\rho(E)$ and E_n may be functions of temperature as well. We have neglected this possibility over the limited temperature range of our measurements.

The cross section $\sigma(h\nu)$ observed at several values of temperature can be fitted with Eq. (11) by using the optical ionization energy $E_n = E_0 + d_{FC}$ and the Franck-Condon shift d_{FC} as adjustable parameters. Since E_0 appears to be of the order of 0.1 eV from thermal measurements,[1] it is clear that the line shape in Fig. 4 can only be fit by Eq. (11) for $d_{FC} \gg E_0$. For if d_{FC} were less than E_0, the cross-section curves would literally disappear from the figures, with σ_{max} occurring at $h\nu \sim 0.2$ eV!

In the limit of a large d_{FC}, the formula for $\sigma(h\nu)$ in Eq. (11) is dominated by the lattice-relaxation Gaussian and the details of the electronic part in Eq. (8) become unimportant. The approximations in Ref. 12 concerning Eq. (8) are therefore perfectly acceptable in this case. A difficulty may arise, however, at $h\nu \gtrsim 1.5$ eV, since above that energy the drop in the crystal density of states[15] at around 2 eV above the conduction-band edge begins to affect the cross section. In order to represent the cross section well at $h\nu \gtrsim 1.5$ eV we would have to abandon our simple model and perform a more rigorous calculation of the electronic part in which the true variation of the electronic matrix element and the density of states farther from the band edge is better accounted for. However, our main objective here

is to determine the magnitude of d_{FC} and E_0 from the thermal broadening and composition dependence of $\sigma(h\nu)$. We are first of all interested in σ between its apparent threshold and maximum, therefore we will take $\rho(E) \propto E^{1/2}$. The theoretical fit for a valence-band-like state, shown in Fig. 4 with the experimental data, was obtained with $d_{FC} = 0.75 \pm 0.1$ eV, $E_0 = 0.10 \pm 0.05$ eV, and $\hbar\omega = 10$ meV. The other parameters were fixed at the values for GaAs ($E_A = 5.2$ eV, $E_F = 11.5$ eV) and $Al_{0.37}Ga_{0.63}As$ ($E_g = 2.05$ eV). This result seems to esentially confirm the original model which we proposed for this center.[1] The thermal and optical energies of the Te-related *DX* center may thus be summarized in Fig. 8(a). The extent to which these data are consistent with a simple CC diagram is shown in Fig. 8(b), where the estimated ranges of error are shown as shaded regions. The values of $E_0 + d_{FC}$ in such a diagram, are quite sensitive to the values chosen for E_∞ and E. However, since the CC diagram is totally determined by only two parameters, we can see that the internal consistency among the data in Fig. 8(b) is quite impressive for so simple a model.

The estimated errors for d_{FC} and E_0 are primarily due to the fact that the experimental data cover only a small range of temperatures. Data at higher temperature would provide a means of testing our model more thoroughly. In addition, it may well be that the linear model is not entirely adequate for such large relaxations. However, the magnitude of the broadening with increasing temperature seems in good accord with the large value of d_{FC} required to fit the shape of $\sigma(h\nu)$ (Fig. 4).

The large value of d_{FC} means that modest variations in the density of states due to variations in composition should not introduce any sharp features in $\sigma(h\nu)$. In particular, the appearance of the tail of low density of states due to the Γ valley being lowered in energy with decreasing x should have no such effect on σ and on the actual position of the level in the gap. We would thus expect that the optical spectrum should be practically unchanged as x increases from 0.4 to 0.6, and should shift only slightly towards lower energies as we move into the direct-gap range. Indeed, this is the behavior of the data in Fig. 5. It occurs because the level does not follow the band edge but rather the higher-lying regions of large density of states primarily associated with the X valley, as indicated in Fig. 9. Any quantitative assessment of the shift of σ towards lower energies with decreasing x is obscured by the large scatter of the data for different compositions. As pointed out in connection with Fig. 6, it would seem that the material contains several Te-related *DX*-type centers of very similar energies and overall properties which may vary somewhat from sample to sample.

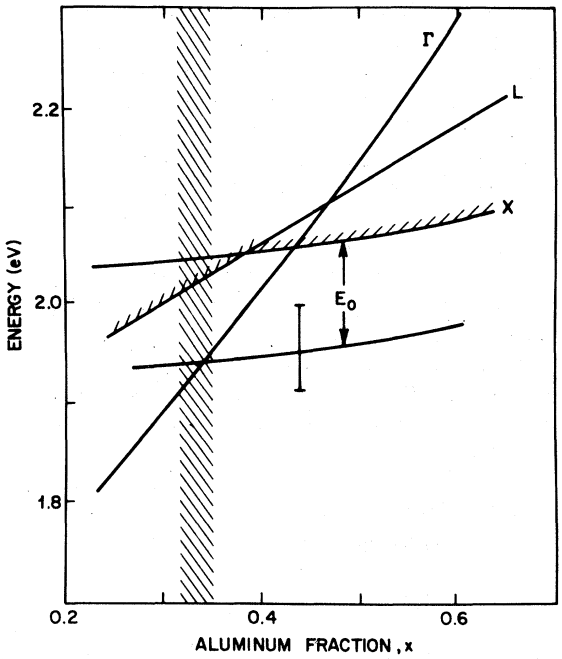

FIG. 9. Equilibrium energy E_0 of *DX* centers in $Al_xGa_{1-x}As$ as deduced from the fit to the optical data in Figs. 4 and 5 with estimated error bar. The shaded region $0.32 < x < 0.35$ indicates the range of composition where E_0 crosses the Fermi level, according to the data in Fig. 7. The lowest high-density-of-states minimum relevant for optical transitions is shown shaded. The $Al_xGa_{1-x}As$ band structure is from Dingle *et al.* (Ref. 16).

In Fig. 9 the range of x where we think E_0 crosses E_F, according to the data in Fig. 7, is shown. The $Al_xGa_{1-x}As$ band structure in Fig. 9 is taken from Dingle *et al.*[16] Unfortunately, it is difficult to know the precise position of the Fermi level in our material. Clearly, that would provide a test of our prediction, for if our result $E_0 = 0.10 \pm 0.05$ eV were correct, the point where the impurity level crosses the Fermi level should occur at a composition x such that the separation between the Fermi level and the bottom of the X valley is on the order of 0.10 eV. With the estimated error of about 50 meV in E_0, we see that the Fermi level must be in the range $-0.05 < E_\Gamma - E_F < +0.05$ eV at $x \simeq 0.33$, to be consistent with these data. Hall data[17,18] on $Al_xGa_{1-x}As$ samples with similar Te concentrations indicate E_F values in this range for the conditions of our measurements. If we can assume that these Hall data were taken on samples with large *DX* concentrations, then the E_D values in Refs. 17 and 18 are a mea-

sure of E_0, as well. For $x>0.5$, where a one-band Hall analysis is valid, the ionization energy extrapolated to low doping levels (which is the appropriate value to compare with optical measurements) is $E_D=0.105$ eV.[18] The estimate of $E_0\sim0.1$ eV in Ref. 1 is also consistent with these values, but is subject to considerable uncertainty since it is the difference of two large numbers.

Thus four independent measurements of E_0—(a) DLTS emission and capture measurements, (b) Hall measurements, (c) the fit to the data of Fig. 4, and (d) the E_F crossing point in Fig. 7—*all* place this equilibrium thermal energy depth between 0.05 and 0.15 eV. This leaves absolutely no doubt as to the reality of the large Stokes shift associated with DX centers.

V. MODEL FOR THE STRUCTURE OF DX CENTERS IN COMPOUND SEMICONDUCTORS

A. Inadequacy of effective-mass theory for deep levels

There are two principal features of the DX-center CC diagram of Fig. 8(b) which are difficult to explain using the traditional views of defect states in semiconductors. They are (a) the extremely large lattice relaxation in which the energy of relaxation d_{FC} is much larger than the apparent binding energy E_0 and (b) the fact that before the capture of an electron the unoccupied DX state is resonant with the conduction band, yet still sufficiently localized to force a lattice relaxation of ~0.75 eV after electron capture.

These apparent inconsistencies can be readily resolved when viewed with our current understanding of deep states in semiconductors. In the past it had always been assumed, in the spirit of the effective-mass theory, that the localization of the wave function could be simply related to the depth of the impurity level in the forbidden gap. Thus the envelope function would be $f\sim\exp(-\alpha r)$, where $\alpha\sim(2m^*E_0)^{1/2}$ in atomic units.[19,20] An effective-mass-like defect state obviously could never be localized if it were resonant with a band. However, if the defect state is properly viewed as arising from many bands and not simply from band states of the nearest minimum, then the degree of localization is no longer related in any simple way to the position of the energy level in the forbidden gap.

In this more general view of deep levels there is no problem in accepting the possibility of a strong lattice relaxation originating from a resonant state, such as the unoccupied DX center. Baraff and Appelbaum[21] have shown that even though a bound state changes discontinuously in character when it moves into the band and becomes a broadened resonance of scattering states, the change in the charge density associated with the potential is continuous. This is a manifestation of the Kohn-Majumdar theorem.[22] According to recent calculations of the energies and wave functions associated with deep states in III-V semiconductors,[12,23,24] it is quite reasonable to expect that a bound state near the conduction-band edge could be sufficiently localized to produce the lattice relaxation required of the DX center. The results of Baraff and Appelbaum allow us to accept such localization for a resonant state as well. Indeed, the DX center might be viewed as an experimental example of the situation described by the Kohn-Majumdar theorem. Of course, we do not intend to imply that a resonant state can ever be truly localized. Indeed, any defect resonance has a delocalized Bloch-wave component in its wave function in addition to a localized component. We define a localized resonant state to be one in which the corresponding electronic charge density is predominantly found in the immediate vicinity of the defect.

When a state is viewed as arising from the overall density of states and not necessarily related in any important way to states at a particular band minimum, we can then understand why $d_{FC}\gg E_0$. This is because the value of E_0 determined for the DX center is not really a measure of the strength of the DX potential, but rather is a measure of the position of the state in the gap with respect to an arbitrary energy reference point, namely the conduction-band minimum at X. In a sense this is the "binding energy", since the net change in free energy necessary to ionize a DX center is E_0. The energy with which d_{FC} should be compared, however, is not E_0, but some measure of the electronic strength of the DX potential. For effective-mass-like defects, these energies are the same, but not for deep levels. For well-characterized deep levels, the Franck-Condon energy is some fraction of the strength of the purely electronic part of the defect potential. For transition elements in GaAs, for example, d_{FC} is of the order of 0.1 E_0,[25] where E_0 in this case is of the order of the intra-d-level crystal-field splitting. Other examples, e.g., ZnO or O in GaP, exhibit values of d_{FC} between 0.1 and 0.5 E_0.[26] Thus our value of $d_{FC}\simeq0.75$ eV would be quite reasonable if the true strength of the DX potential were of the order of 2 eV. In this context, also, the 60 meV range of energies in Fig. 6, which seems large compared to the equilibrium depth of $E_0\sim0.1$ eV or the thermal-emission depth of $E\sim0.3$ eV, is almost negligible if the DX center is considered to have a potential strength of ~2 eV.

B. Discussion of *DX* model

We have seen above that the apparently peculiar properties of the *DX* center need not be considered at all unusual when viewed within the non-effective-mass framework of deep levels. Indeed, based on recent state-of-the-art computer calculations of deep levels,[12,23,24] there exists a very common and plausible type of defect which exhibits all of the qualitative features of the *DX* center, namely, the donor-anion-vacancy complex. In fact, *any* complex containing an anion vacancy is dominated by this defect and has properties qualitatively similar to the isolated vacancy. Thus any complex of an anion vacancy plus an impurity or even a divacancy (alone or with an impurity) will behave roughly like an anion vacancy. The model which we will propose is merely the simplest form of donor-vacancy complex. The data do not preclude more complicated anion-vacancy-related defects.

The unrelaxed As vacancy in GaAs has a gap of ~2 eV between the a_1 and t_2 states which are available for the dangling electrons, as shown schematically in Fig. 10.[24] This splitting is a measure of the strength of the V_{As} potential and is the energy with which d_{FC} ~0.75 eV should be compared. Calculations of impurity-vacancy complexes[24] show that the presence of the impurity, e.g., a Te-donor atom, does not strongly affect the overall properties of the complex, which is still basically V_{As}-like both in its energy and wave function. The similarity between isolated vacancies and impurity-vacancy complexes, as well as the insensitivity of such complexes to the details of the impurity potential, are well known experimentally for cation-vacancy complexes.[27,28] Indeed, the existence of the donor-cation-vacancy complex has been very well established; it is the so-called self-activated luminescence center in II-VI semiconductors.[28] Anion vacancies or their complexes, on the other hand, have not been unambiguously identified except in a few very wide-gap II-VI compounds such as BeO, ZnO, and ZnS.[28] This is consistent with the theoretical picture in which the much stronger potential at the anion site pushes the anion-vacancy levels farther up from the valence band than is the case for the cation vacancy. Thus in all but the wider-gap materials, the anion vacancy and its associated complexes have deep states originating in the valence band and pushed all the way up through the gap and into the conduction band, i.e., these valence-band-like anion-vacancy states are deeper than E_g. In those materials where these highly localized states are located near the edge of the conduction band, it is possible to have *DX*-like behavior with the unoccupied level resonant with the conduction band, while the occupied level relaxes to a bound state in the gap. Such is the essence of persistent photoconductivity.

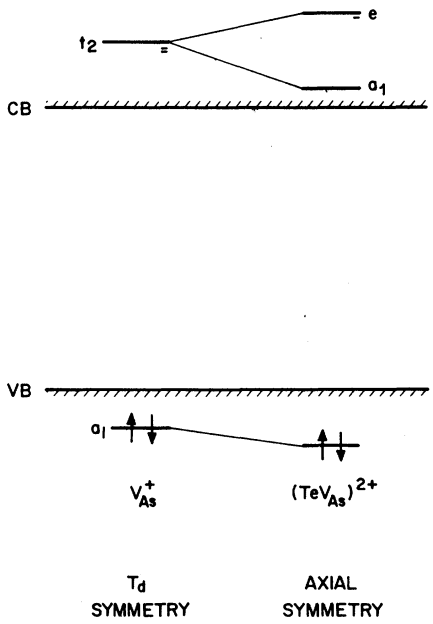

FIG. 10. Schematic single-electron energy-level diagram for the unrelaxed positive arsenic vacancy and Te V_{As}^{2+} complex in GaAs and $Al_xGa_{1-x}As$. The relative ordering of the a_1 and e states of Te V_{As} depends on the sign of the axial distortion. Note that the energies shown are intended to be of only qualitative significance.

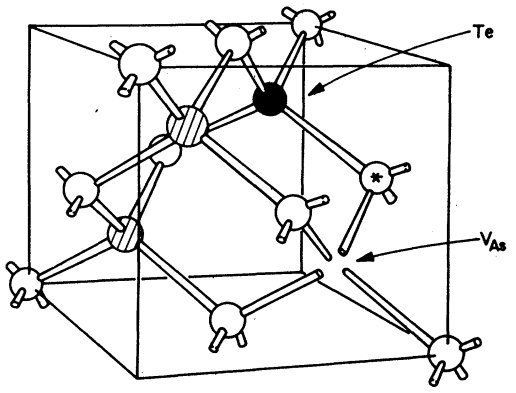

FIG. 11. Crystal model of one of the 12 equivalent second-nearest-neighbor positions for the Te donor in the simplest form of Te V_{As} complex in $Al_xGa_{1-x}As$. The As atoms are shown shaded with the Ga(Al) atoms plain. The Ga(Al) atom marked by an asterisk moves in response to the Te donor and hence produces the axial distortion of the vacancy. Different locations of the Te donor and/or different local Al-Ga distributions are likely to produce the range of *DX* energies observed in Fig. 6. Sn or Si donors occupy Ga sites which are first nearest neighbors of the As vacancy and hence give rise to shifted *DX* energies, as explained in the text.

Thus, we propose a model in which the microstructure of DX-like centers is a complex involving a donor and an anion vacancy. An example of one possible donor-anion-vacancy complex is shown for Te donors in $Al_xGa_{1-x}As$ in Fig. 11. Experimental data, of course, can never actually prove that such a model is correct, but within the general trends that have emerged from the recent calculations of native defects and deep impurities in III-V compounds[12,23,24,29] our proposal is the only defect model among those which have been studied which is consistent with the observations.

Let us first briefly discuss the other defect models which have been theoretically analyzed in order to show that they cannot even qualitatively explain the DX-center data, i.e., they cannot produce a "deep" highly localized state above the conduction-band edge in $Al_xGa_{1-x}As$. We will consider substitutional chemical impurities, antisite defects cation-vacancy complexes, and interstitials.

None of the substitutional chemical impurities and/or their pairs appear to be likely candidates. Deep levels due to most chemical defects have been found in the gap. Even in cases where the electronegativity difference between the host and impurity atoms is large (i.e., ZnTe:O, GaP:O), a level exhibiting lattice relaxation appears in the forbidden gap.[23] The exceptions are transition-metal elements and perhaps the elements from the rare-earth groups. However, these are known to exhibit only small Stokes shifts and their behavior is generally determined by the d and f character of their incomplete shells.

An antisite defect, if it exists, should behave as a simple double donor or acceptor, since it has only a weak short-range potential.

The gallium vacancy and its complexes have weak potentials and are expected to produce levels in the gap.[24] Such a level has been observed in electron-irradiated $Al_xGa_{1-x}As$ and identified as being due to V_{Ga}.[30] The donor-V_{Ga} complexes are apparently the source of the well-known 1.2-eV luminescence band in As-rich GaAs.[27]

Very little is known about interstitials, especially bonded interstitials. Impurity interstitials generally behave as shallow effective-mass donors, but self interstitials have never been identified in semiconductors, except as close-pair Frenkel defects in ZnSe.[28]

Let us now discuss the behavior of the Te-V_{As} model of Fig. 11 vis-á-vis the DX centers in Te-doped $Al_xGa_{1-x}As$, keeping in mind that the actual defect structure might differ somewhat in detail from that shown but still be dominated by V_{As}. The attractive donor potential will lower the symmetry of V_{As} and split the triply degenerate t_2 state as shown in Fig. 10. The position of these energy levels may vary perhaps within a few tenths of a volt or so with different chemical donors or donor locations, but the overall properties are determined by the symmetry and by the strength of the vacancy potential. The shifts in E_0 due to different donors, as well as the ~60 meV fluctuations in the energy of the Te-complex in Fig. 6, are consistent with this expectation. Indeed, the experimental donor-related shifts seen in the donor-V_{Zn} self-activated luminescence centers in ZnS and ZnSe are also 40–50 meV.[27] According to the extrapolation of Fig. 9, the donor-V_{As} complexes as well as isolated V_{As} should be located well up into the conduction band in pure GaAs, and are thus relatively inactive electrically. This may explain the relative weakness of the recovery stage apparently associated with V_{As} in irradiated GaAs.[31]

It is natural to ask whether this defect model is adequate to explain the persistent-photoconductivity centers seen in other materials, i.e., S-doped $GaAs_{1-x}P_x$,[32] S-doped GaSb,[33] and Cl- and Ga-doped $Cd_{1-x}Zn_xTe$,[34] and CdTe.[35-37] Since we would expect most anion vacancies in III-V and II-VI compounds to give rise to states near the conduction-band edge for material with E_g in the general vicinity of 2 eV, the model proposed here should be suitable to explain all such data (except perhaps GaSb with its very small gap, where V_{Ga} could be near the conduction band). The relatively small differences in the strength of the interactions and their effect on the actual position of the energy levels may have important consequences, however. In particular, if the states originating from the t_2 levels associated with the vacancy are not pushed as deeply into the conduction band as in Fig. 10 or 12(a), one of the levels might be in the gap and the complex might show acceptor behavior, as indicated in Fig. 12(b). Indeed, the defects in $GaAs_{1-x}P_x$ (Ref. 32) and $Cd_{1-x}Zn_xTe$ (Ref. 34) exhibit an increase in mobility after photoexcitation, i.e., behave as acceptors. On the other hand, the DX center in Te-doped $Al_xGa_{1-x}As$ is a donor by virtue of a decrease in mobility after excitation.[5] We would expect from our model, in agreement with experiment[32] that the DX center in $GaAs_{1-x}P_x$ should be an acceptor since V_P in GaP produces a state in the gap[29] and hence is like Fig. 12(b). Thus in wide-gap materials like GaP or CdS we would not expect to find DX-like high-mobility persistent-photoconductivity behavior, for in those cases the anion-vacancy potential is not strong enough to push the state above, or as far as, the conduction-band edge, and the DX center should behave like a normal deep level in the gap. This again is consistent with experiment, for persistent photoconductivity

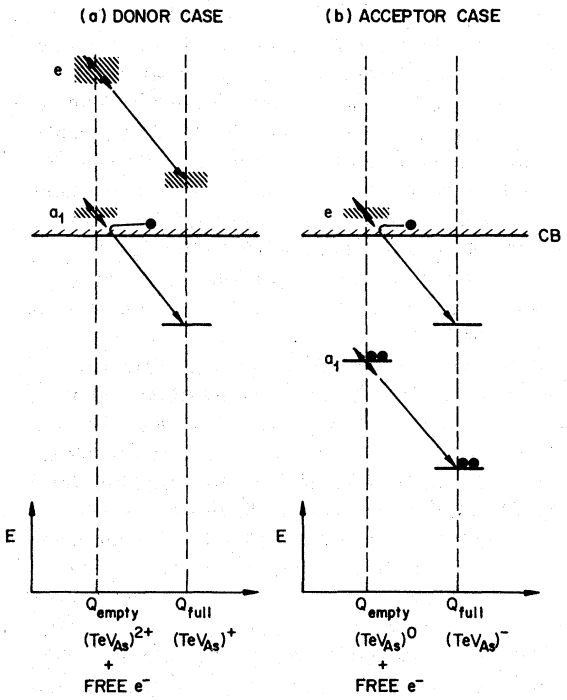

FIG. 12. Schematic single-electron energy-level diagrams of Te V_{As} showing the possibility of either donor (a) or acceptor (b) behavior depending on the position of the axially split a_1 and e states relative to the edge of the conduction band.

has not been seen in GaP. In CdS the persistent-photoconductivity state exhibits extremely low mobility[38] and most likely involves impurity-banding effects, and not defect centers which are resonant with the conduction band.

Very large relaxation effects, defined by a CC diagram such as Fig. 8(b), in which $d_{FC} = S\hbar\omega > E_0$, are of course quite common in ionic materials. The well-known carrier self-trapping phenomenon in these materials is a typical example. Another more recent example is that of In in CdF_2.[39] This along with the *DX* centers in III-V compounds, might be considered an example of what Toyozawa calls the *extrinsic* self-trapping of an electron.[40] Even though the microscopic models of the various defects may be quite different in these very different materials, there seems to be a general trend in which defects exhibit either relatively small or very large relaxation with few, if any, intermediate cases. This behavior has, in fact, been predicted on very general theoretical grounds for strongly coupled electron-lattice systems.[41,42] The *DX* centers are thus striking evidence that such behavior, which had been largely confined to ionic materials, also exists in the rather covalent III-V semiconductor compounds as well.

C. Other proposed V_{AS} identifications

We must now deal with the fact that our proposed V_{As}-impurity-complex model for the *DX* center is in apparent conflict with the assignment of V_{As}-related defect complexes to particular GaAs photoluminescence lines in the vicinity of 1.4 eV.[27,43] Most of these assignments are highly speculative, but the recent ion implantation experiments of Itoh and Takeuchi[43] seem to give good evidence for the luminescence line at 1.4 eV being due to Si-V_{As}. We believe, however, that this assignment cannot possibly be correct. The main argument against this identification is that this defect is observed to form during the 500-K recovery stage of electron-irradiated GaAs:Si when Ga-displacement-produced native defects, e.g., V_{Ga} and As_{Ga}, are mobile.[30,31] In particular, the 1.4 eV line forms during the λ_2 substage, which is associated with the motion of the defect, or defects, responsible for the shallow $E1$ and $E2$ electron traps.[31] It has been suggested[30] that these levels might be the two states of the As_{Ga} antisite defect, which should be a relatively shallow double donor. In any event, they are certainly not due to V_{As}, which is thought to become mobile during the recovery stages at 235 and 280 K.[31]

How, then, do we explain the observation of Itoh and Takeuchi[43] that As^+ ion implantation reduces the 1.4 eV luminescence while Ar^+ implantation does not. These data are clear evidence that the concentration of the defect responsible for the 1.4 eV line is depressed by excess arsenic. Conversely, the increase in this line within 1 μm of the surface as a result of high-temperature annealing treatments, is consistent with the defect concentration being enhanced by an arsenic deficiency. While the above data are certainly consistent with the defect in question involving V_{As}, they are also equally consistent with the defect involving Ga_i, Ga_{As}, or any chemical impurity which is substitutional on an arsenic site. Watkins[28] has shown for ZnSe (which in many ways is very similar to GaAs) that the vacancies and vacancy-impurity complexes which have been identified by EPR typically have very broad optical line shapes. He specifically points out that one should not expect any vacancy-related defect to produce sharp luminescence lines. This is consistent with our assertion that the relatively sharp 1.4 eV luminescence line is not related to an arsenic vacancy.

We believe that the most reasonable model for the defect giving rise to the 1.4 eV line is a Si_{As} acceptor, plus whatever it is which gives the ($E1$, $E2$) deep-level pair, perhaps As_{Ga}. This would explain the 500-K annealing data[31] as well as the

implantation data of Itoh and Takeuchi,[43] since then the As^+ implantation can be seen to diminish the 1.4 eV line by reducing the Si_{As} concentration due to a suppression of the V_{As} concentration. The tendency for an As_{Ga} double donor and Si_{As} acceptor to pair would be substantial because of their strong Coulomb attraction. Indeed, the ($E1, E2$) defect shows a strong tendency during the 500-K stage to pair with acceptors, e.g., Cd and Zn.[31] Thus, we believe that the stoichiometric arguments for the identification of V_{As} and its complexes are weak and at best ambiguous, with alternate explanations possible which are equally valid. When we consider additional factors such as the damage-rate orientation dependences, the optically induced EPR in related materials, and the expected quantum-mechanical properties of vacancy-related states, we see that the donor-V_{As} model is most appropriate for the DX center and not the sharp 1.4 eV luminescence line in GaAs.

VI. CONCLUSIONS

The electron photoionization cross section σ_n^0 of DX centers in Te-doped $Al_xGa_{1-x}As$ has been measured as a function of temperature and composition by the photocapacitance technique. The line shape and temperature dependence of $\sigma_n^0(h\nu)$ can be consistently fit by a phonon-broadened line-shape theory and can imply a considerable lattice relaxation associated with the capture or emission of an electron at the defect. The best fit is for an equilibrium depth $E_0 = 0.10 \pm 0.05$ eV with a relaxation energy $d_{FC} = S\hbar\omega = 0.75 \pm 0.1$ eV. This is consistent with the large-lattice-relaxation model for persistent photoconductivity which we have recently proposed. This fact, together with the evidence discussed in Ref. 1, leaves very little doubt that such a model correctly describes the overall qualitative features of the DX centers, which give rise to persistent-photoconductivity effects in a number of III-V and II-VI semiconductors.

In addition to the optical data, we presented data on the variations of the DLTS signal due to the DX centers both as a function of Al fraction x and applied stress. These data locate the composition range where the occupied DX energy level crosses the Fermi level in our samples at approximately $0.32 < x < 0.35$. This, along with estimates of the position of E_F from Hall data on similar samples in the literature, is in reasonable agreement with the value of E_0 determined from the optical fit.

From an analysis of TSCAP and photocapacitance data we find that the concentration of DX centers in our samples is large—about ten times the normal net shallow-donor-concentration N_D in most samples, and typically within the range $1 < N_{DX}/N_D < 30$. Thus, since the DX center is itself a donor, it is usually the dominant donor in Te-doped $Al_xGa_{1-x}As$. In Te-doped samples the DX concentration is roughly proportional to the Te concentration. Doping with Se gives the same effect as Te. In samples doped with Sn or Si, on the other hand, a different but closely related type of DX center is produced, again proportional to the donor concentration. These observations are strong evidence that the DX center involves a donor atom, hence the "D" of DX.

Finally, we have argued that the verification of the model of Ref. 1 forces us to assume that a defect state exists which is resonant with the conduction band when unoccupied, but which relaxes to a point nearly 0.8 eV deep in the gap after the capture of an electron. Thus the defect wave function must be sufficiently localized, even when it is a resonance in the continuum states of the band, to produce a very substantial lattice relaxation. We believe that the existence of such a state supports the view, based on recent calculations, that the localization of a deep-level wave function is not necessarily related to the position of the corresponding energy level in the forbidden gap. This is contrary to the picture of defect wave functions in semiconductors based on the effective-mass theory.

Based on experience gained from recent computer calculations of the energies and wave functions of various native defects and chemical impurities in III-V compounds, we believe that the simplest consistent model for the microstructure of DX-type defects is a complex involving a donor and an anion vacancy. For the case of Te-doped $Al_xGa_{1-x}As$ which we are studying, this corresponds to Te-V_{As}. We propose that such a model for the structure of DX centers may be quite valid in general and can explain the data on persistent photoconductivity and other effects due to DX centers in a number of III-V and II-VI semiconductors.

ACKNOWLEDGMENTS

We wish to acknowledge the assistance of H. G. White and A. J. Williams, who have been instrumental in growing, processing, and testing the dozens of samples used in this study. Special thanks are due Ann Silversmith who took much of the photocapacitance data. We have also benefited from various stimulating discussions with our colleagues, in particular, V. Narayanamurti, G. A. Baraff, M. Schluter, C. H. Henry, J. L. Merz, and J. P. van der Ziel. One of us (M. J.) would like to thank ONR for their partial support under Contract No. N00014-76-0890.

*Present address: Dept. of Theor. Phys., The University, Newcastle Upon Tyne, U. K.
[1]D. V. Lang and R. A. Logan, Phys. Rev. Lett. 39, 635 (1977).
[2]G. L. Miller, D. V. Lang, and L. C. Kimerling, Ann. Rev. Matl. Sci. 7, 377 (1977).
[3]D. V. Lang, J. Appl. Phys. 45, 3023 (1974).
[4]G. L. Miller, IEEE Trans. Electron Devices 19, 1103 (1972).
[5]R. J. Nelson, Appl. Phys. Lett. 31, 351 (1977).
[6]C. T. Sah and V. G. K. Reddi, IEEE Trans. Electron Devices 11, 345 (1964).
[7]G. Goto, S. Yanagisawa, O. Wada, and H. Takanashi, J. Appl. Phys. 13, 1127 (1974).
[8]K. Hesse and H. Strack, Solid-State Electron. 15, 767 (1972).
[9]D. L. Losee, Appl. Phys. Lett. 21, 54 (1972); J. Appl. Phys. 46, 2204 (1975).
[10]H. G. Grimmeiss, Ann. Rev. Matl. Sci. 7, 341 (1977).
[11]D. E. Aspnes, Phys. Rev. B 14, 5331 (1976).
[12]M. Jaros, Phys. Rev. B 16, 3694 (1978).
[13]K. Huang and R. Rhys, Proc. R. Soc. 204, 406 (1950).
[14]T. H. Keil, Phys. Rev. 140, A601 (1965).
[15]J. R. Chelikowsky and M. L. Cohen, Phys. Rev. B 14, 556 (1976).
[16]R. Dingle, R. A. Logan, and J. R. Arthur, Jr., *GaAs and Related Compounds (Edinburgh)*, 1976 (Inst. Phys. Conf. Ser. No. 33a, 1977), p. 210.
[17]A. J. SpringThorpe, F. D. King, and A. Becke, J. Electron. Mat. 4, 101 (1975).
[18]Yu. E. Maronchuk and N. A. Yakuseva, Fiz. Tekh. Poluprovodn. 10, 1349 (1976) [Sov. Phys. Semicond. 10, 800 (1976)].
[19]W. Kohn, Solid State Phys. 5, 259 (1957).
[20]V. Heine and C. H. Henry, Phys. Rev. B 11, 3795 (1975).
[21]G. A. Baraff and J. A. Appelbaum, Phys. Rev. B 5, 475 (1972).
[22]W. Kohn and C. Majumdar, Phys. Rev. 138, A1617 (1965).
[23]M. Jaros, J. Phys. C 8, 2455 (1975).
[24]M. Jaros and S. Brand, Phys. Rev. B 14, 4494 (1976).
[25]J. I. Pankove, *Optical Processes in Semiconductors*, (Prentice-Hall, Englewood Cliffs, 1971), p. 142.
[26]C. H. Henry and D. V. Lang, Phys. Rev. B 15, 989 (1977).
[27]E. W. Williams and H. B. Bebb, in *Semiconductors and Semimetals*, edited by R. K. Willardson and A. C. Beer (Academic, New York, 1972), Vol. 8, p. 321.
[28]G. D. Watkins, *Radiation Effects in Semiconductors*, 1976 (Inst. Phys. Conf. Ser. No. 31, 1977), p. 95.
[29]M. Jaros and G. P. Srivastava, J. Phys. Chem. Sol. 38, 1399 (1977).
[30]D. V. Lang, R. A. Logan, and L. C. Kimerling, Phys. Rev. B 15, 4874 (1977).
[31]D. V. Lang, *Radiation Effects in Semiconductors*, 1976 (Inst. Phys. Conf. Ser. No. 31, 1977), p. 70.
[32]M. G. Craford, G. E. Stillman, J. A. Rossi, and N. Holonyak, Jr., Phys. Rev. 168, 867 (1968).
[33]A. Ya. Vul', L. V. Golubev, L. V. Sharonova, and Yu. V. Shmartsev, Fiz. Tekh. Poluprovodn. 4, 2347 (1970) [Sov. Phys. Semicond. 4, 2017 (1971)]; L. Dmowski, M. Baj, M. Kubalski, R. Piotrzkowski, and S. Porowski, Fourteenth International Conference on the Physics of Semiconductors, Edinburgh, 1978 (to be published).
[34]B. C. Burkey, R. P. Khosla, J. R. Fischer, and D. L. Losee, J. Appl. Phys. 47, 1095 (1976).
[35]M. R. Lorenz, B. Segall, and H. H. Woodbury, Phys. Rev. 134, A751 (1964).
[36]H. F. MacMillan, Ph.D. Thesis (Stanford University, 1972) (unpublished).
[37]G. W. Iseler, J. A. Kafalas, A. J. Strauss, H. F. MacMillan and, R. H. Bube, Solid State Commun. 10, 619 (1972).
[38]H. C. Wright, R. J. Douney, and J. R. Canning, J. Phys. D 1, 1593 (1968).
[39]U. Piekara, J. M. Langer, and B. Krukowska-Fulda, Solid State Commun. 23, 583 (1977).
[40]Y. Toyozawa, Proceedings of the International Conference on Recombination in Semiconductors, Southampton, 1978 (to be published).
[41]A. Sumi and Y. Toyozawa, J. Phys. Soc. Jpn. 35, 137 (1973).
[42]D. Emin and T. Holstein, Phys. Rev. Lett. 36, 323 (1976).
[43]T. Itoh and M. Takeuchi, Jpn. J. Appl. Phys. 16, 227 (1977) and references therein.